Environmental Pollution 245 (2019) 627–633

Contents lists available at ScienceDirect

Environmental Pollution

journal homepage: www.elsevier.com/locate/envpol

Geographical detection of groundwater pollution vulnerability and hazard in karst areas of Guangxi Province, China☆

Zhen Zhu [a, 1], Jiaxin Wang [b, d, 1], Maogui Hu [b, e, *], Lin Jia [c, **]

[a] Guangxi Geoenvironmental Monitoring Station, Guilin 530023, China
[b] State Key Laboratory of Resources and Environmental Information System, Institute of Geographic Sciences and Natural Resources Research, Chinese Academy of Sciences, Beijing, 100101, China
[c] Beijing Municipal Research Institute of Environmental Protection, Beijing 100037, China
[d] University of Chinese Academy of Sciences, Beijing 100049, China
[e] Jiangsu Center for Collaborative Innovation in Geographical Information Resource Development and Application, Nanjing 210023, China

ARTICLE INFO

Article history:
Received 15 July 2018
Received in revised form
27 September 2018
Accepted 2 October 2018
Available online 9 October 2018

Keywords:
PLEIK
Geodetector
Covered karst area
Vulnerability assessment
Hazard assessment

ABSTRACT

Groundwater pollution is a critical concern in karst areas. This study used the PLEIK (P: protective cover; L: land use; E: epikarst development; I: infiltration conditions; K: karst development) method to assess the vulnerability of groundwater pollution in Guangxi Province, which is the largest karst area in China. The pollution sources and attenuation consist of groundwater pollution hazards. The attributions for the vulnerability and hazard were measured using the geodetector method from geographical information system in Luzhai County in Guangxi. The results confirmed that the vulnerability of groundwater pollution was higher in karst areas than in non-karst areas. In Guangxi, 36.35% of the groundwater samples were polluted. A total of 49.73% of the areas in Luzhai County contained hazardous levels of pollution. The risk assessment map, which interacted with the vulnerability and hazards, was 58.2% similar to the groundwater pollution distribution. The influence of the hazard on groundwater pollution was 2.6 times that of the vulnerability. It is crucial to control pollution sources to prevent groundwater pollution.

1. Introduction

Karst is a specific type of terrain that develops over limestone and dolomite due to the dissolution of carbonate rocks from erosion and subsequent physicochemical processes (Zwahlen, 2003; Darnault, 2008). The soil layers of karst areas in southwest China are thin with a surface-ground bilayer structure, which makes it easy for pollutants to enter aquifers through the weak overlying strata and sinkholes (Li et al., 2018). Once contaminated, karst groundwater resources are difficult to salvage without expending significant efforts and costs (Zwahlen, 2003; Wang et al., 2012; Guo et al., 2007). Groundwater contamination in karst areas has become an increasingly critical issue. Intrinsic vulnerability, hazard and risk assessments are crucial tools to ensuring groundwater protection (Wang et al., 2012; Zhang et al., 2016).

The intrinsic vulnerability of groundwater is determined by the geological and hydrogeological characteristics of an area. Intrinsic vulnerability is, however, independent of the contaminants' nature and scenario (Zwahlen, 2003). Because the karst groundwater system has a complicated structure, diverse types of karst areas have different hydrological characteristics (Zou et al., 2014). One of the most widely used intrinsic vulnerability models is DRASTIC, which is a generic model built by the US EPA that incorporates various physical components of both aquifers and the overlying substrate (Beynen et al., 2012). The DRASTIC method has some limitations when applied to karstic aquifers due to the surface-ground bilayer structure in karst areas (Polemio et al., 2009). Because the conduit network and the connected joints and fractures divide a more compact zone of limestone in karst areas, the EPIK method was developed for karst aquifers by taking the karst network into consideration (Hamdan et al., 2016). European approaches for the protection of karst groundwater were developed

☆ This paper has been recommended for acceptance by Dr. J Rinklebe.
* Corresponding author. State Key Laboratory of Resources and Environmental Information System, Institute of Geographic Sciences and Natural Resources Research, Chinese Academy of Sciences, Beijing, 100101, China.
** Corresponding author.
E-mail addresses: humg@lreis.ac.cn (M. Hu), jl_0706@163.com (L. Jia).
[1] The equal first authors and equal contributions.

https://doi.org/10.1016/j.envpol.2018.10.017
0269-7491/

in the COST Action 620 project, where the COP method first assessed the vulnerability of karst regions based on an origin-pathway-target model (Entezari et al., 2016). The EPIK model can be applied to the bare karst area in South China, which has a rich karst surface zone and network, whereas the COP model better suits North China's shallow buried karst area with a weak karst surface zone (Zou et al., 2014). The PLEIK model was the best fit for examining the covered karst in China because it highlighted protective cover and land use patterns (Zou et al., 2014; Wen et al., 2016; Dai et al., 2015).

Hazard assessment quantifies the potential degree of harmfulness for each type of hazard and is determined using the toxicity and quantity of dangerous substances (Zwahlen, 2003). There are three methods for such an assessment. First is the spatial analysis of the positions and types of pollution, including those from overlying and buffer sources (Li et al., 2018; Kazakis et al., 2015). Alternatively, the weighted sum model accounts for the different parameters of pollution sources, including land use, pollutant amounts, toxicity, and mobility (Bai et al., 2012; Zhang et al., 2016). Finally, the product model takes not only the attributes of pollution sources into consideration but also their attenuation, infiltration, technical status, and control policy (Li et al., 2017; Andreo et al., 2006; Shrestha et al., 2016; Wang et al., 2012). The parameters of each method are adjustable according to the available data.

As vulnerability and hazard assessment methods become more widely used, doubts have increased regarding their applicability, accuracy, and reliability (Wang et al., 2012; Iván and Mádl-Szőnyi, 2017). Few researchers have validated assessment results. Shrestha et al. (2016) used Pearson's *r* correlation coefficient to perform a statistical comparison of the vulnerability and risk using an observed nitrate level. The results indicated that the correlation coefficient is positive for risk and negative for vulnerability. Cui et al. (2016) contrasted the pollution risk and distribution maps qualitatively, which displayed a coherent distribution. Li et al. (2017) identified inconsistencies in the relationship between the risk map and organic contamination. However, the explanatory power of the vulnerability and pollutant sources for groundwater pollutant concentration is still relatively unexplored.

In this study, the PLEIK method was used to assess the vulnerability of covered karst areas in southwestern China. We evaluated the hazard map of pollutant sources using the geostatistical method from geographical information science. Utilizing the CCME WQI method (Wang et al., 2018), we then evaluated the groundwater pollutant classes based on the field sampling. Finally, the geographical detector method (Wang et al., 2010) was used to quantitatively evaluate the relationships between the groundwater pollution classes, the vulnerability, and the hazard. The results revealed the explanatory power of the vulnerability, the hazard, and their interactions concerning groundwater pollution, which should greatly aid groundwater protection and management efforts.

2. Material and methods

2.1. Study area

Guangxi Province lies in southern China and occupies a total area of 236.7 thousand square kilometres. It spans from 20.90° N to 26.38° N in latitude and 104.47° E to 112.07° E in longitude under a subtropical monsoon climate (Fig. 1). In Guangxi, there are large areas of well-developed tropical karst landscape from the northeast to the southwest. The aquifer rock formations are divided into five categories, including loose rock formations, pure carbonate rock formations, impure carbonate rock formations, clastic rock formations, and intrusive rock formations. Correspondingly, the types of groundwater in Guangxi contain pore water in loose rock, pore water in clastic rock, fissure-cavern water, and bedrock fissure water. The main source of groundwater is precipitation; however, other sources exist, including the river water supply, irrigation sources, and other miscellaneous water sources in the karst area. Groundwater in Guangxi is shallow freshwater and is mainly used in industrial and agricultural production as well as domestic drinking water. Therefore, it is crucial to protect groundwater from pollution.

2.2. Data

There were a total of 1029 field samples that were used to evaluate the groundwater pollution in Guangxi Province (Fig. 1). The analysis indexes had 30 items, including 8 inorganic indicators (NH4+, As, Cd, Cr6+, Pb, Hg, NO2- and NO3-), 2 organic indicators (trichloromethane and tetrachloromethane), 16 volatile indicators (1,1,1-trichloroethane, trichloroethylene, tetrachloroethylene, 1,2-dichloroethane, 1,1,2-trichloroethane, 1,2-dichloropropane, tribromomethane, chloroethylene, 1,1-dichloroethylene, chlorobenzene, o-dichlorobenzene, p-dichlorobenzene, methylbenzene, ethylbenzene, xylene and styrene) and 4 semi-volatile indicators (BHC, γ—BHC, DDT and HCB). These samples covered all hydrogeological units in the study area, which controlled the main underground rivers and karst springs in the basin.

2.3. Methods

2.3.1. PLEIK

The vulnerability of covered karst areas were assessed using five factors: protective cover (P), land use (L), epikarst development (E), infiltration conditions (I) and karst development (K).

P encompasses all geotechnical layers above the groundwater table, including the overlying non-karst strata and karst strata above the groundwater table. In karst areas, P has a significant defensive effect against pollution. Once pollutants get through the protective cover, they quickly and heavily contaminate the groundwater. One of the most important parameters for the

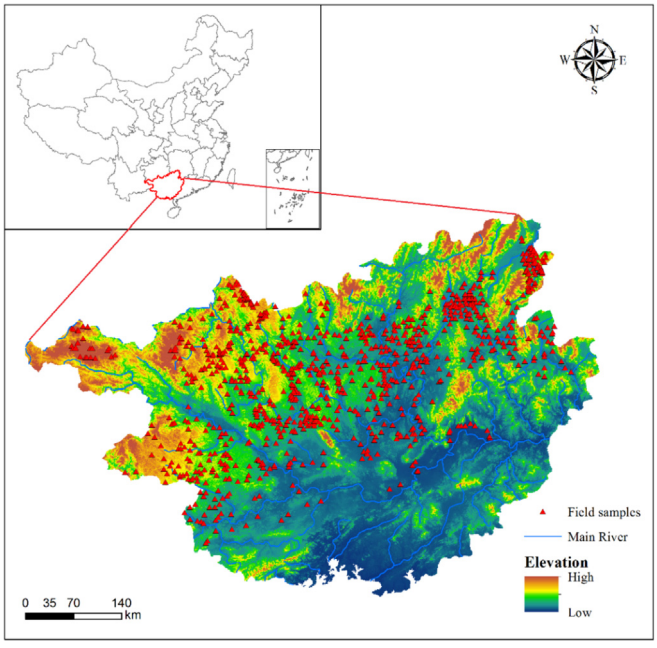

Fig. 1. Study area and field samples distribution.

protective cover is the soil thickness. The thinner the protective cover's soil, the more vulnerable the covered karst area becomes. The soil thickness was divided into four categories (Table 1). Another crucial attribute of the protective cover is the degradation ability of the soil. The stronger the degradation ability is, the lower the vulnerability. The cation exchange capacity (CEC) was selected as a proxy to reflect the protective cover's degradation ability. The soil thickness and CEC were connected to quantify the protective cover's effectiveness using a rating matrix (Table 1).

L incorporates the impacts of human activities on covered karst areas into a vulnerability assessment. More human activity leads to higher vulnerability. Land use was divided into six classes and scored (Table 1).

E is located under any consolidated soil (Doerfliger et al., 1999) and has important pondage action for karst water systems. A number of factors—including the lithology, rock structure, and hydrodynamic conditions—can affect its development. More highly developed epikarst contributes to a higher vulnerability rating. Epikarst development can be measured and scored based on its specific type of carbonate rocks (Table 1).

I concerns the recharge type and recharge intensity (RI) of the karst aquifer. The more concentrated the recharge and the larger the intensity, the higher the vulnerability. The recharge type depends on the slope and its vegetation, which we classified into four categories (Table 1). Like the soil thickness and CEC, we also quantified the infiltration conditions using a rating matrix based on the recharge type and intensity (Table 1).

K is a network of solution openings greater than 10 mm in diameter. This size is the effective minimum aperture for turbulent flow (Doerfliger et al., 1999). Groundwater runoff moduli can be used to reflect the karst development of an aquifer. The smaller the modulus, the stronger the karst network development, which results in a higher vulnerability (Table 1).

The vulnerability index (VI) was generated using the weighted sum of five factors (Eq. (1)).

$$VI = w_1{*}P + w_2{*}L + w_3{*}E + w_4{*}I + w_5{*}K \quad (1)$$

P, L, E, I, and K serve as the factors' scores. Lower scores indicate higher vulnerability. $w_1, w_2, w_3, w_4, and\ w_5$ are the respective weights for each factor, and the fuzzy comprehensive evaluation method determines each weight (Zou et al., 2014). Equation (2) illustrates the final weighted vector.

$$w = (0.29, 0.24, 0.20, 0.16, 0.11) \quad (2)$$

Each factor's score—and, essentially, the range of VI—fell in the range of 1–10. The vulnerability was then divided into five classes (Table 1). Lower values correspond to higher vulnerability.

Table 1
Classifications and scores of P, L, E, I, K and VI.

	Class	Protective cover thicknesses		Score matrix (CEC (meq/100 g))			
		A	B	<10	10~100	100~200	>200
P	P_1	0–20 cm	0–20 cm	1	3	5	7
	P_2	20–100 cm	20–100 cm	2	4	6	8
	P_3	100–150 cm	100 cm	3	5	7	9
	P_4	>150 cm	>100 cm or non-karst strata	4	6	8	10

L	**Class**	**Land use**	**Score**
	L_1	Forest	10
	L_2	Grass land	8
	L_3	Garden land	6
	L_4	Farmland	4
	L_5	Bare land	2
	L_6	Urban and industrial land	1
E	**Class**	**Epikarst development**	**Score**
	E_1	Limestone continuum	1
	E_2	Limestone with dolomite	3
	E_3	Limestone dolomite interaction	5
	E_4	Impure carbonate	7
	E_5	Impure and non-carbonate interaction	9
	E_6	Non-carbonate	10

	Class	**Infiltration conditions**				**Score matrix (RI(mm/d))**		
		C (m)	**D (m)**	**E**	**F**	<9.9	10–24.9	>25
I	I_1	2000	2000	–	–	4	2	1
	I_2	2000–4000	2000–4000	>10%	Farmland	6	4	3
				>25%	Grassland			
	I_3	2000–4000	–	<10%	Farmland	8	6	5
				<25%	Grassland			
	I_4	The rest of the catchment				10	8	7

K	**Class**	**Moduli ($L{\cdot}s^{-1}{\cdot}km^{-2}$)**	**Score**
	K_1	<1	1–3
	K_2	1–7	4–5
	K_3	7–15	6–8
	K_4	>15	9–10
VI	**Class**	**Vulnerability Degree**	**Score**
	VI_1	Higher	1–2
	VI_2	High	2–4
	VI_3	Medium	4–6
	VI_4	Low	6–8
	VI_5	Lower	8–10

Notes: A = Soil covered on the limestone; B= Soil covered on low permeability bottom; C= Sinkhole; D = Subterranean stream; E = Slope; F= Vegetation.

2.3.2. CCME WQI

To evaluate the groundwater, we used the CCME WQI method to integrate the parameters into a single index (Eq. (3)). The index ranges from 0 (worst water quality) to 100 (best water quality) (Wang et al., 2018).

$$\text{CCME WQI} = 100 - \frac{\sqrt{F_1^2 + F_2^2 + F_3^2}}{1.732} \quad (3)$$

Here, F_1 is the percentage of indicators that do not meet the standard limits at least once, F_2 represents the percentage of field samples that do not meet the standard limits, and F_3 represents the average excess multiple for each sample (Terrado et al., 2010; Wang et al., 2018). In this study, the CCME WQI was used to calculate the integrated pollution concentration of the field samples. The pollution samples were defined as those whose monitoring indicators exceeded the national standard of class III for groundwater quality. The standard limits used in the formula were the national standard for groundwater quality of class III (GBT 14,848–2017). For the classification, the range of categories can be modified for each case study (Terrado et al., 2010). In this study, the CCME WQI values have been divided into five categories: poor (0–44), marginal (44.1–64), fair (64.1–79), good (79.1–99.9) and no pollution (100).

2.3.3. Geographical detector

The geographical detector method proposed by Wang et al. (2010, 2016; 2018) was used to compare the spatial consistency of the vulnerability, hazard, and risk maps versus the pollution concentrations in field samples. Higher similarity in the spatial distribution increases the reliability of the assessment map. The factor detector can be used to evaluate these similarities (Eq. (4)). If the assessment map can reflect the actual vulnerability and risk, the variance in the samples' pollution within strata is less than that between the strata.

$$q = 1 - \frac{\sum_{h=1}^{L} N_h \sigma_h^2}{N\sigma^2} \quad (4)$$

L represents the number of strata. N_h represents the total number of field samples in stratum h, and N is the total number of field samples in the population. σ_h^2 and σ^2 represent the variances. The value of q is within [0,1]. The larger the value, the stronger the explanatory power of the assessment map.

The natural environment's inherent vulnerability and the hazardous pollution from human activities directly and interactively influence groundwater pollution. The interactive detector can help evaluate the interaction (Table 2). $q(X1 \cap X2)$ represents the interactive explanatory power of the vulnerability and hazard assessment maps on groundwater pollution.

3. Results and discussion

3.1. Vulnerability assessment

Factor P considered the protective cover's permeability, soil thickness, and CEC. In the study area, most soil covered the limestone directly, and so the P class was determined by the soil thickness according to Table 1. For coastal areas in southern Guangxi, the soil type was latosol with a thickness of more than 1.5 m, which falls in category P_4. Latosol is also a heavy clay soil with strong adsorption, meaning that the CEC is low—less than 5 meq/100 g. According to Table 1, the P score for these areas is 4. For the southern subtropics in central Guangxi, the soil type was latored soil with a thickness of less than 1.5 m, which falls in category P_3. The CEC here lies between 5 and 10 meq/100 g, which grants these areas a P score of 3. Red soil with a thickness of less than 1 m comprises the main soil type in the low hills of central and northern Guangxi and in the southern high altitude areas reaching 350–800 m. In mid-mountain zones with an altitude of 800–1300 m, the soil type is mountainous yellow soil—also with a thickness of less than 1 m. The Nanling mountainous region (at an altitude of 1400–1800 m) has a mountain yellow brown soil type with a thickness of less than 1 m. For the karst area in Guangxi, the soil type is limestone soil, which has a thickness between 0.3 and 0.4 m. Those areas all belong to category P2. The CEC is more than 10 meq/100 g. Therefore, the P score for those areas is 4. There are small areas in the northeast of Guangxi whose soil type is meadow soil, which has a thickness of less than 0.1 m. They belong to category P1. The CEC is more than 10 meq/100 g. Therefore, the P score for the areas is 3. Fig. 2(A) shows the final classification for factor P in the study area.

Factor L signifies the land use type. Forested regions—which are mainly distributed in the north, east and southwest—cover 116,147 square kilometres, or 48.89%, of the total study area. Farmland takes second place with 42,471 square kilometres, which occupies 17.88% of the total area. Grassland areas cover 28,944 square kilometres, which comprises 12.18% of the study area. Most study areas have grass lands. Bare land covers 23,518 square kilometres and comprises 9.90% of the total area, and it is most common in the central western areas. Urban and industrial land covers 9097 square kilometres and comprises 3.8% of the total area. Finally, garden land covers 5088 square kilometres and comprises 2.14% of the total area. Fig. 2(B) shows the final classification for factor L in the study area.

Factor E considered the type of carbonate rocks. Limestone continuum, limestone with dolomite, and limestone dolomite interaction are classified as pure carbonate rocks, and the impure carbonate interlayer is less than 10% of the total. The E scores were 1, 3 and 5. Impure carbonate and non-carbonate interaction occur in epibolite. The former has an impure carbonate interlayer that is more than 50% of its total and a non-carbonate interlayer that is less than 15% of its total, such as the carbonate rocks with clasolite. The latter has an impure carbonate interlayer that is more than 50% of its total and a non-carbonate interlayer that is more than 30% of its total, such as sandstone, conglomerate and igneous rock. The E scores were 7 and 9. Non-carbonate includes shale and mudstone with scores of 10. Fig. 2(C) shows the final classification for factor E in the study area.

Factor I considered the recharge type and intensity. The I classes in the study area were divided based on the results in Table 1. The recharge intensity refers to the average rainfall per day. In the study area, precipitation occurs more frequently in the eastern hills towards the windward slopes than in the western basin area on the leeward slopes. According to local weather stations, the average daily rainfall was less than 9.9 mm. In Table 1, the scores of classes I_1, I_2, I_3, and I_4 were 4, 6, 8, and 10, respectively. Fig. 2(D) shows the final classification for factor I in the study area.

Factor K considered the groundwater runoff modulus. The modulus in most areas measured between 7 and 15 $L \cdot s^{-1} \cdot km^{-2}$, which was less than 1 in the limestone areas. The classes of factor K were divided into K_1, K_2, K_3, and K_4 and the scores were 3, 5, 8 and 10, respectively. Fig. 2(E) illustrates the final classification for factor K in the study area.

The VI was generated using a weighted sum of these five factors. The scores ranged between 2 and 10. The vulnerabilities were then divided into four classes according to Table 1. Fig. 2(F) shows the final vulnerability assessment map. As expected, the vulnerabilities in most areas of Guangxi can be classified as low. The karst area, however, has high vulnerability, as shown in Fig. 2(F).

Table 2
Interaction relationships for two factors.

Description	Interaction
$\mathbf{q}(\mathbf{X1}\cap\mathbf{X2}) < \mathbf{Min}(\mathbf{q}(\boldsymbol{X1}), \mathbf{q}(\mathbf{X2}))$	Weaken, nonlinear
$\mathbf{Min}(\mathbf{q}(\boldsymbol{X1}), \mathbf{q}(\mathbf{X2})) < \mathbf{q}(\mathbf{X1}\cap\mathbf{X2}) < \mathbf{Max}(\mathbf{q}(\boldsymbol{X1}), \mathbf{q}(\mathbf{X2}))$	Weaken, uni-
$\mathbf{q}(\mathbf{X1}\cap\mathbf{X2}) > \mathbf{Max}(\mathbf{q}(\boldsymbol{X1}), \mathbf{q}(\mathbf{X2}))$	Enhance, bi-
$\mathbf{q}(\mathbf{X1}\cap\mathbf{X2}) = \mathbf{q}(\boldsymbol{X1}) + \mathbf{q}(\mathbf{X2})$	Independent
$\mathbf{q}(\mathbf{X1}\cap\mathbf{X2}) > \mathbf{q}(\boldsymbol{X1}) + \mathbf{q}(\mathbf{X2})$	Enhance, nonlinear

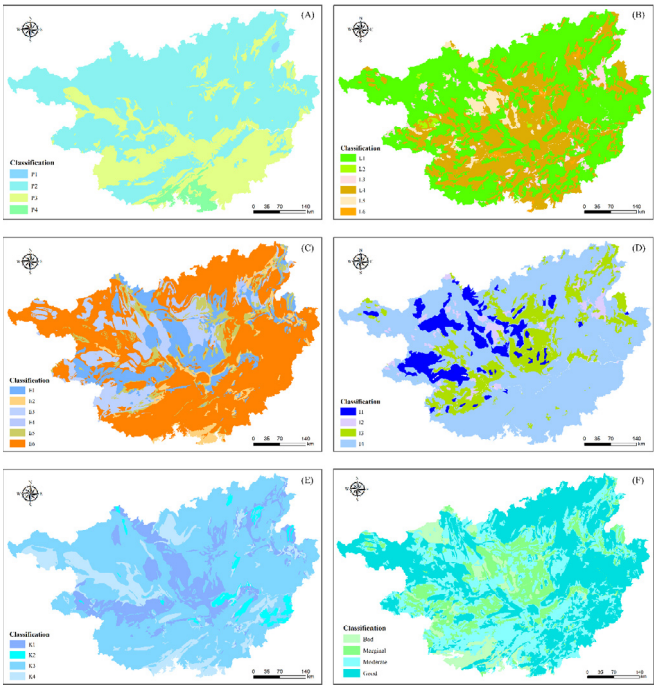

Fig. 2. Classifications for the P, L, E, I, and K factors and the vulnerability assessment results.

3.2. Hazard assessment of groundwater pollution

In this study, the pollution sources were collected from 2011 to 2014. The categories of analysis included industrial, mineral, agricultural, and domestic pollution sources. There were a total of 249 pollution sources, including 99 industrial and mineral pollution sources, 46 domestic pollution sources, and 104 agricultural pollution sources. The sources spanned 28 counties but were mostly concentrated in the northeastern portion of the study area. The pollution sources in other countries were not available. Luzhai County contained 28 pollution sources in total and was selected to assess the hazard (Fig. 3).

Buffer analysis in geographical information system was used to evaluate the influence degrees of pollution sources. The influence scopes and intensities were scored according to the types of pollution sources (Table 3). Longer distances from pollution sources lessened the influence degree of the pollution. The scores were added up when more than one pollution source overlapped (Li et al., 2018).

The hazard in Luzhai County was assessed using a buffer analysis method. The pollution sources' influence in adjacent counties was also considered. As shown in Fig. 4, the hazard was divided into five classes: very low, low, moderate, high, and very high. Areas out of the buffer zone were defined as no hazard areas. Statistically, 50.23% of areas had no hazard and 42.08% had very low hazard. Other pollution classes made up less than 10% of the samples. They were 4.64%, 2.18%, 0.54% and 0.33% for the classes of low, moderate, high and very high, respectively. The pollution degree for Luzhai County was optimistic.

3.3. Integrated groundwater pollution

Using the CCME WQI method, we combined the different indicators into one index. A total of 30 indicators were integrated, including 8 inorganic regular indexes, 2 organic regular indexes, 16 volatile organic compound non-regular indexes and 4 semi-volatile organic compound non-regular indexes. The groundwater standard of class III was used as the standard limit to evaluate the excess multiple and the pollution degree while considering the pollution type and load simultaneously. Table 4 lists the name of each indicator and their standard limit.

From a total of 1029 field samples, 374 exceeded the class III groundwater standards. The main pollutant indicators included NH4+, As, Cd, Pb, Hg, NO2-, NO3- and HCB. A total of 306 samples were polluted only by one excessive item, 63 samples were polluted by two items, and there were 5 samples polluted by three items simultaneously. HCB was the highest indicated pollutant and was found in 213 samples. Heavy metal pollution (Hg, Cd, Pb and As) was less, and its components polluted just 2, 2, 12 and 17 samples, respectively.

Fig. 5 displays the samples' pollutant classes, which were calculated using the CCME WQI method. A total of 655 samples were not contaminated and comprised 63.65% of the total samples. A total of 309 samples belonged to pollution class IV and were slightly polluted. Fifty-nine samples belonged to pollution class III and were moderately polluted. Four samples belonged to pollution class II and were heavy polluted. Only 2 samples belonged to pollution class I and were severely polluted. In general, the pollution is less in the study area. The pollutant samples mostly lied in the karst area where the vulnerability was high.

3.4. Explanatory power evaluation

The geodetector method was used to evaluate the explanatory power of the hazard and vulnerability assessment maps for groundwater pollution in Luzhai County. For groundwater pollution that is measured using the CCME WQI, the q values for the hazard and vulnerability assessment maps were 0.378 and 0.144,

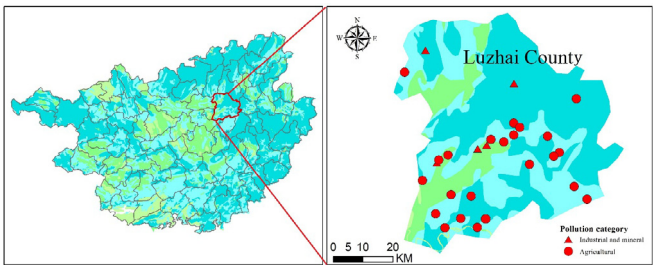

Fig. 3. Pollution source distribution in Luzhai County.

Table 3
Influence scopes and scores of pollution sources.

Category	Influence scopes	Scores
Industrial and mineral pollution source	0–2000 m	3
	2000–4000 m	2
	4000–6000 m	1
Agricultural pollution source	0–2000 m	5
	2000–4000 m	3
	4000–6000 m	1
Domestic pollution source	0–2000 m	8
	2000–4000 m	5
	4000–6000 m	2

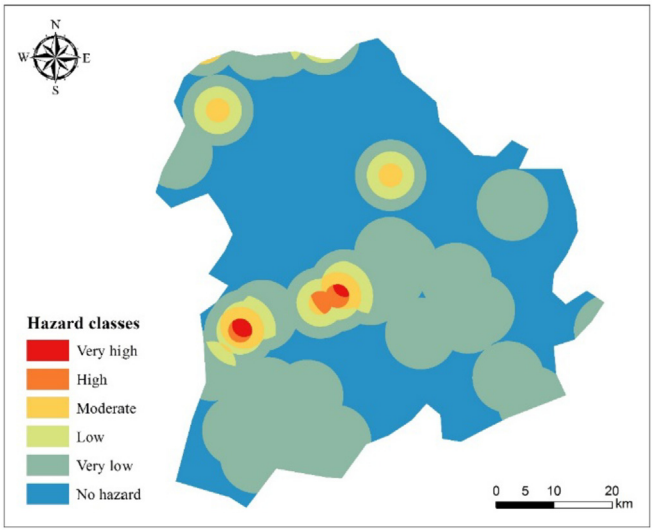

Fig. 4. Hazard assessment map for study area.

Table 4
Indicators and standard limits.

Category	Name	Standard limit
Inorganic (mg/L)	NH4+	0.05
	As	0.01
	Cd	0.005
	Cr6+	0.05
	Pb	0.01
	Hg	0.001
	NO2−	1
	NO3-	20
Organic (μg/L)	Trichloromethane	60
	Tetrachloromethane	2
Volatile (μg/L)	1,1,1-Trichloroethane	2000
	Trichloroethylene	70
	Tetrachloroethylene	40
	1,2-Dichloroethane	30
	1,1,2-Trichloroethane	5
	1,2-Dichloropropane	5
	Tribromomethane	100
	Chloroethylene	5
	1,1-Dichloroethylene	30
	Chlorobenzene	300
	o-Dichlorobenzene	1000
	pDichlorobenzene	300
	Methylbenzene	700
	Ethylbenzene	300
	Xylene	500
	Styrene	20
Semi-volatile (μg/L)	BHC	5
	γ-BHC	2
	DDT	1
	HCB	1

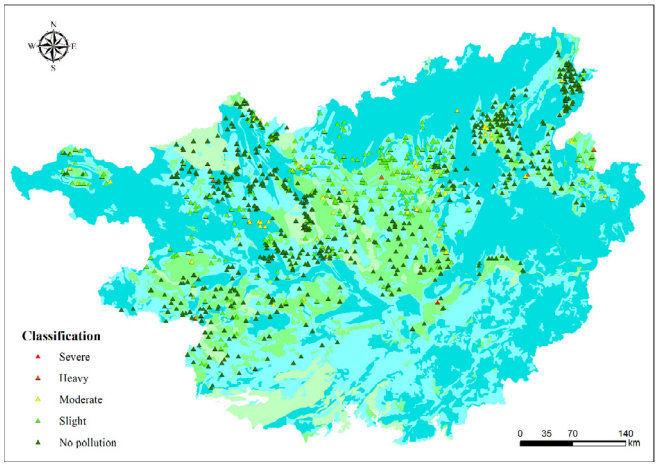

Fig. 5. Classification of the field samples.

respectively. The combined value of hazard and vulnerability was 0.582, which is a nonlinear enhancement based on Table 2.

Groundwater pollution was determined both by the aquifer's intrinsic characteristics—which were relatively static—and the existence of potentially polluting activities—which were dynamic and easily controlled (Saidi et al., 2010; Saidi et al., 2011; Wang et al., 2012). For the polluting activities, various types of pollution sources were selected in the study, including industrial and mineral pollution sources, domestic pollution sources, and agricultural pollution sources. These pollution sources released different kinds of compounds, which caused the groundwater pollution. For example, industrial and mineral pollution sources typically release heavy metals, such as As, Cd, Cr6+, Pb, and Hg. The domestic pollution sources include NH4+, NO2-, and NO3-. The agricultural pollution sources mainly released organic compounds and heavy metals. Although there might be other compounds released by the pollution sources, which were not assessed in the study, the most important compounds have been included and taken into consideration in the study area. The explanatory power for the hazard and vulnerability assessment maps indicated that hazard influenced groundwater pollution 2.6 times more than vulnerability. Hazard was generated by human activities, while vulnerability reflected the intrinsic attributes of the hydrogeological characteristics (Andreo et al., 2006). These results confirm the importance of controlling human impacts on groundwater protection efforts.

On the other hand, the explanatory power also evaluated the effectiveness of the hazard and vulnerability assessment maps. The hazard assessment results had a 37.8% similarity with groundwater pollution, whereas the vulnerability assessment results had a 14.4% similarity. With respect to their combined effect, the hazard and vulnerability assessment had a 58.2% similarity with groundwater pollution. The explanatory power was in high contrast to former research (Shrestha et al., 2016). Other studies (Torres et al., 2018; Alfy et al., 2017) have also researched the influence of hydrogeological and anthropogenic factors on groundwater pollution. The main influential factors in various areas were different, depending on the geology types, the types of pollutants, the evaluation methods and so on. Han et al. (2016) reviewed the contamination of water pollution in China and indicated that the major sources of groundwater pollution included municipal and industrial wastewater discharge and agricultural fertilizers, which were the crucial pollution sources that were considered in this article when assessing the hazard. Due to the limited available data, the hazard assessment only considered the types of pollution sources and the damping effect with distance. Sudden natural

catastrophes, inconsistent operating procedures (Li et al., 2017), and the pollutant amounts and toxicity (Bai et al., 2012; Zhang et al., 2016) could also generate hazards. There may be some impact on the explanatory power of the hazard assessment results. More detailed data could be used to further assess the explanatory power of hazard on groundwater pollution.

4. Conclusions

For the vulnerability assessment, the PLEIK method effectively assessed the vulnerability in covered karst areas, which highlighted the importance of protective cover and land use. While assessing the hazard of groundwater pollution, 50.23% of the areas in Luzhai County displayed no hazard. A total of 36.35% of the groundwater samples were polluted in the study area. The geodetector method evaluated the vulnerability and hazard assessment maps and assessed their explanatory power for groundwater pollution quantitatively. The explanatory power for the hazard and vulnerability assessment maps showed that they have a combined 58.2% similarity with actual groundwater pollution. Hazard influenced groundwater pollution 2.6 times more than vulnerability. These results suggest that controlling pollution sources is more crucial and more effective to prevent groundwater pollution than reducing vulnerability.

Funding

This work was supported by the National Natural Science Foundation of China (grant numbers 41771434 and 41531179), the National Science and Technology Major Project (grant numbers 2017ZX10201302 and 2017YFA0604804), and the Innovation Project of LREIS (grant number O88RA200YA).

Declarations of interest

None.

References

Alfy, M.E., Lashin, A., Abdalla, F., Al-Bassam, A., 2017. Assessing the hydrogeochemical processes affecting groundwater pollution in arid areas using an integration of geochemical equilibrium and multivariate statistical techniques. Environ. Pollut. 229, 1–11.

Andreo, B., Goldscheider, N., Vadillo, I., Vías, J.M., Neukum, C., Sinreich, M., et al., 2006. Karst groundwater protection: first application of a Pan-European Approach to vulnerability, hazard and risk mapping in the Sierra de Líbar (southern Spain). Sci. Total Environ. 357 (1-3), 54–73.

Bai, L., Wang, Y., Li, F., 2012. Research on gis-based risk assessment method of groundwater pollution and its application. Adv. Mater. Res. 356–360, 819–824.

Beynen, P.E.V., Niedzielski, M.A., Bialkowska-Jelinska, E., Alsharif, K., Matusick, J., 2012. Comparative study of specific groundwater vulnerability of a karst aquifer in central Florida. Appl. Geogr. 32 (2), 868–877.

Cui, Y., J., He, Wang, M., Zhao, Y., Wang, F., 2016. Exploration of risk assessment method towards groundwater contamination in karst region:a case study in Disu underground river system basin. Carsol. Sin./Zhong Guo Yan Rong 35 (4), 372–383.

Dai, C., Li, H., Pan, Z., Zhao, S., Huang, S., 2015. Comparison of the REKST model with PLEIK model in performing the antifouling analysis of karstic groundwater:a case study in the Xiangxi Dalongdong underground river. Carsol. Sin./Zhong Guo Yan Rong 34 (4), 354–361.

Darnault, C.J.G., 2008. Karst aquifers: hydrogeology and exploitation. In: Darnault, C.J.G. (Ed.), Overexploitation and Contamination of Shared Groundwater Resources. Springer Netherlands, pp. 203–226.

Doerfliger, N., Jeannin, P.Y., Zwahlen, F., 1999. Water vulnerability assessment in karst environments: a new method of defining protection areas using a multi-attribute approach and GIS tools (EPIK method). Environ. Geol. 39 (2), 165–176.

Entezari, M., Yamani, M., Aghdam, M.J., 2016. Evaluation of intrinsic vulnerability, hazard and risk mapping for karst aquifers, khorein aquifer, kermanshah province: a case study. Environmental Earth Sciences 75 (5), 1–10.

Guo, Q., Wang, Y., Gao, X., Ma, T., 2007. A new model (DRARCH) for assessing groundwater vulnerability to arsenic contamination at basin scale: a case study in Taiyuan basin, northern China. Environ. Geol. 52 (5), 923–932.

Hamdan, I., Margane, A., Ptak, T., Wiegand, B., Sauter, M., 2016. Groundwater vulnerability assessment for the karst aquifer of Tanour and Rasoun springs catchment area (NW-Jordan) using COP and EPIK intrinsic methods. Environmental Earth Sciences 75 (23), 1474.

Han, D., Currell, M.J., Cao, G., 2016. Deep challenges for China's war on water pollution. Environ. Pollut. 218, 1222–1233.

Iván, V., Mádl-Szőnyi, J., 2017. State of the art of karst vulnerability assessment: overview, evaluation and outlook. Environmental Earth Sciences 76 (3), 112.

Kazakis, N., Oikonomidis, D., Voudouris, K.S., 2015. Groundwater vulnerability and pollution risk assessment with disparate models in karstic, porous, and fissured rock aquifers using remote sensing techniques and GIS in Anthemountas basin, Greece. Environmental Earth Sciences 74 (7), 6199–6209.

Li, B., Zeng, Y., Zhang, B., Wang, X., 2018. A risk evaluation model for karst groundwater pollution based on geographic information system and artificial neural network applications. Environmental Earth Sciences 77 (9), 344.

Li, H., Yu, X., Zhang, W., Ying, H., Yu, J., Zhang, Y., 2017. Risk assessment of groundwater organic pollution using hazard, intrinsic vulnerability, and groundwater value, Suzhou city in China. Exposure & Health 10 (2), 1–17.

Polemio, M., Casarano, D., Limoni, P.P., 2009. Karstic aquifer vulnerability assessment methods and results at a test site (Apulia, southern Italy). Natural Hazards & Earth System Sciences & Discussions 9 (4), 1461–1470.

Saidi, S., Bouri, S., Dhia, H.B., 2010. Groundwater vulnerability and risk mapping of the Hajeb-jelma aquifer (central Tunisia) using a GIS-based drastic model. Environmental Earth Sciences 59 (7), 1579–1588.

Saidi, S., Bouri, S., Dhia, H.B., Anselme, B., 2011. Assessment of groundwater risk using intrinsic vulnerability and hazard mapping: application to souassi aquifer, tunisian sahel. Agric. Water Manag. 98 (10), 1671–1682.

Shrestha, S., Semkuyu, D.J., Pandey, V.P., 2016. Assessment of groundwater vulnerability and risk to pollution in kathmandu valley, Nepal. Sci. Total Environ. 556, 23–35.

Terrado, M., Barceló, D., Tauler, R., Borrell, E., Campos, S.D., Barceló, D., 2010. Surface-water-quality indices for the analysis of data generated by automated sampling networks. Trac. Trends Anal. Chem. 29 (1), 40–52.

Torres, N.I., Xue, Y., Padilla, I.Y., Macchiavelli, R.E., Ghasemizadeh, R., Kaeli, D., et al., 2018. The influence of hydrogeological and anthropogenic variables on phthalate contamination in eogenetic karst groundwater systems. Environ. Pollut. 237, 298–307.

Wang, J., He, J., Chen, H., 2012. Assessment of groundwater contamination risk using hazard quantification, a modified drastic model and groundwater value, beijing plain, China. Sci. Total Environ. 432 (16), 216–226.

Wang, J., Hu, M., Zhang, F., Gao, B., 2018. Influential factors detection for surface water quality with geographical detectors in China. Stoch. Environ. Res. Risk Assess. (4), 1–13.

Wang, J., Li, X., Christakos, G., Liao, Y., Zhang, T., Gu, X., Zheng, X., 2010. Geographical detectors-based health risk assessment and its application in the neural tube defects study of the Heshun Region, China. Int. J. Geogr. Inf. Sci. 24 (1), 107–127.

Wang, J., Zhang, T., Fu, B., 2016. A measure of spatial stratified heterogeneity. Ecol. Indicat. 67, 250–256.

Wen, Y., Lu, L., Zhao, L., Zhao, K., 2016. Study on groundwater pollution risk assessment in Chongqing. Environmental Pollution & Control 38 (3), 90–98.

Zhang, B., Li, G., Cheng, P., Yeh, T.C.J., Hong, M., 2016. Landfill risk assessment on groundwater based on vulnerability and pollution index. Water Resour. Manag. 30 (4), 1465–1480.

Zou, S., Li, L., Lu, H., Liu, Q., Su, C., Zhu, D., 2014. The vulnerability assessment method of karst groundwater. Acta Geosci. Sin. 35 (2), 262–268.

Zwahlen, F., 2003. Vulnerability and risk mapping for the protection of carbonate (karst) aquifers. European Commission, Directorate-General XII Science, Research and Development, Brussels, p. 297.